DIHADRON CORRELATIONS AND FLOW

Leonora Vesterbacka Olsson

Lund University
Sweden

Supervised by Peter Christiansen

September 6, 2013

Abstract

This thesis treats two methods for the computation of the flow found in Quark Gluon Plasma produced in lead-lead collisions at $\sqrt{s_{NN}} = 2.76\,\text{TeV}$ with the ALICE detector at the LHC. The results provided by the two methods show dominant elliptic and triangular flow measured for central collisions, as well as di-jets originating from hard collisions.

Contents

Introduction

Since its formulation in the 1960's, the Standard Model has been the leading theory explaining the smallest constituents of matter. It has gained success for being experimentally tested at high level of accuracy and its ability to describe three out of four forces of nature. Albeit its success, there are still many unresolved issues. Questions like: How does matter behave at extreme temperatures? Can the quarks inside the protons and neutrons be deconfined? are hopefully answered in the study of heavy ion collisions and the elusive Quark Gluon Plasma (QGP). This thesis will treat the phenomenon of *flow* found in heavy ion collisions, considered to prove the existence of the Quark Gluon Plasma. The study of flow will be done by analyzing particle distributions obtained in lead-lead collisions at the Large Hadron Collider at CERN. Two recently proposed methods will be used and their results will be stated and compared. The two methods are compared and any deviation will be explained by either a physical component or shortcomings in the methods.

Chapter 1: Theory

This section contains an overview of central concepts of modern particle physics, such as the Standard Model and Quantum Chromodynamics (QCD), as well as an introduction to the phenomena of Quark Gluon Plasma. These theories are crucial in understanding the concept of heavy ion collisions, and the content of the subsequent chapter concerning flow.

The Standard Model

The dominant theory in particle physics from the second half of the last century until today has been the Standard Model (SM). According to the Standard Model, matter consists of elementary particles which interact through three types of fundamental forces. The model is effective in sorting the composite particles after their properties such as spin, charge and mass. The elementary particles are divided into subgroups with either half-integer spin, the quarks and leptons, or with integer spin, the force mediators. The known quarks, leptons and force mediators are presented in Figure 1. The leptons carry electric charge and the quarks carry both electric charge and the so called color charge.

The force mediators of the Standard Model are bosons and account for three of the four forces of nature, where the fourth force, gravity, is not included. The mediator of the electromagnetic interaction, the photon, interacts with particles that possess electromagnetic charge. The rigorous theory explaining this interaction is called Quantum Electrodynamics (QED). The mediators of the weak force, the Z^0 and the $W^\pm$ bosons, can interact with all fermions. The mediators of the strong force, the gluons, interact with particles that possess color charge, i.e quarks and gluons. Hadrons are composite particles made up of quarks and gluons, collectively called partons. The hadrons can be either baryons, consisting of three

quarks, or mesons consisting of a quark anti-quark pair, both with neutral color charge.

Figure 1: The Standard Model of elementary particles. There are three columns for the three generations (I, II, III) containing two quarks and leptons each, as well as an additional column for the force mediators. [10]

QCD

Quantum Chromodynamics (QCD) is the theory describing the strong force and its properties. In QCD, the gluons couple to color charge analogously to the way photons couple to electromagnetic charge in QED. Despite this apparent similarity, the gluons possess features that will make the behaviour of QCD far more complicated than QED. The most obvious distinction is that the gluons carry a non-zero color charge enabling them to interact with each other. Through quantum fluctuations, the gluons can emit and absorb new gluon pairs, this emission and absorption results in an anti-screening of the original gluon charge, i.e an increase of the force at large distance.

Asymptotic freedom and confinement are other unique features of QCD. Experimentally, all observed particles are color charge neutral, and it is generally believed that there can be no free quarks. In contrast to the electromagnetic interaction, the strong interaction increases with larger quark separation. The gluons counteract the separation of quarks, to prevent isolated color charges. This phenomenon is called confinement. Contrary to the electromagnetic interaction, the strong force is weaker at short distances. The strong interaction appears weak for distances of the order of the quark separation inside a hadron. This makes the quarks inside a hadron to appear free, or asymptotically free.

The above mentioned features of the strong interaction are explained by a running coupling constant α_s, that varies drastically over different ranges of energy, being constant at high energies, and increasing at lower energies. The coupling constant is presented in

Figure 2 as a function of the resolution energy Q. Perturbation theory is an essential calculation tool in particle physics, but since the coupling constant cannot be treated in a perturbative way when it gets large, calculations in low energy QCD become impossible.
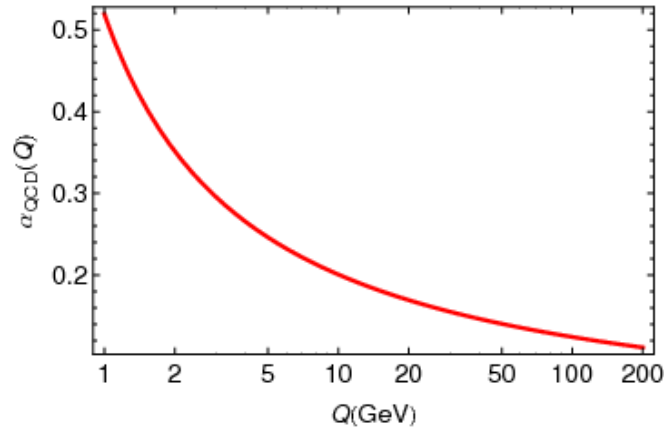

Figure 2: The strong coupling constant is large for low energies and decreases for higher energies, where Q is the resolution scale. [17]

Inside hadrons, the total momentum will be shared by all the partons, according to a certain parton distribution function, which is defined as the probability density for finding a particle with a certain longitudinal momentum fraction x at resolution scale Q^2 [9]. This means that there are partons that carry a large fraction of momentum, as well as a small fraction. In heavy ion collisions, the ions themselves consist of a large number of partons, resulting in a wide distribution of the parton momenta. According to Figure 2, the partons carrying a large fraction of momenta will interact through external particles with a small coupling constant, whereas those carrying a small fraction will interact through external particles with a large coupling constant.

Quark-Gluon Plasma

Starting from the phenomena of color confinement and asymptotic freedom found in QCD, one can propose an admixture of the two features called deconfinement. As the name suggests, deconfinement is the opposite of confinement. Unlike the "free" quarks and gluons inside a hadron due to asymptotic freedom, in deconfinement this freedom can extend outside to larger distances if the surrounding properties are right. This occurs for high energy densities, where the hadrons become dissolved and their constituents mixed, resulting in a new state called the Quark Gluon Plasma (QGP), presented in a phase diagram in Figure 3. It has been proposed that this QGP state was dominant in the universe during the first few microseconds after the Big Bang. By studying QGP, one brings understanding to the early

evolution of the universe. This high density state of matter possesses properties similar to those found in hydrodynamics. This means that one can treat collisions with many participating partons as a fluid characterized by collective properties, rather than as a gas of solid billiard balls.
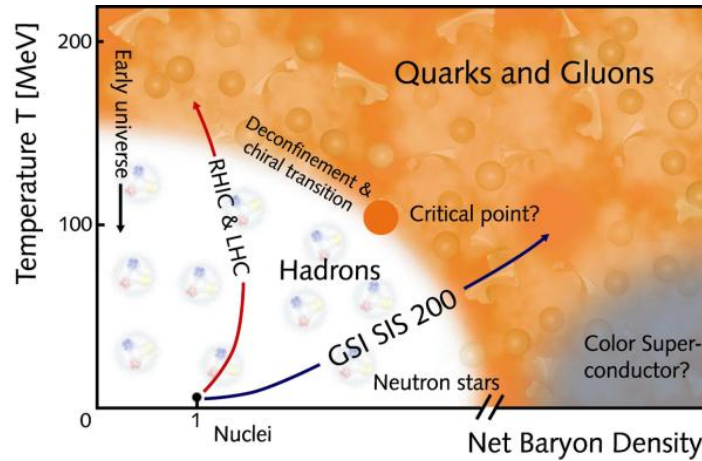

Figure 3: A diagram presenting the onset of the QGP phase at high temperatures and high baryon densities. [14]

Chapter 2: Heavy Ion Collisions

Heavy Ion Collisions (HIC) research at energy densities high enough to possibly produce QGP has been conducted at the SPS accelerator at CERN, the RHIC at Brookhaven National Laboratory and recently at the LHC at CERN. By colliding heavy and highly energetic nuclei, such as lead and gold, one can study the collective effects of the formed medium. The dynamic evolution of the compound system of a heavy ion collision can be characterized in different stages.

Prior to the collision, the nuclei are Lorentz contracted due to the relativistic energies. When the two nuclei collide, there are two possibilities for interactions. The partons carrying a large fraction of momentum will react as asymptotically free particles. The collisions between these partons are called hard collision and produce "hard-particles", such as hadronic jets, dilepton pairs and heavy quarks. The partons carrying a small fraction of momentum can be characterized as a bulk medium due to the large coupling constant. The interactions in this soft region provide a large number of soft collisions, leading to quark anti-quark and gluon pair creation. The partons that do not form new hadrons will start to interact with each other in this hot dense medium. The parton-soup resembles a fluid as it approaches thermal equilibrium. After about $1\,\mathrm{fm/c}$, it is estimated that the partonic matter enters the QGP phase. The jets produced from hard collisions will traverse the plasma and thus

lose energy. For an anisotropy in the geometrical shape of the plasma, the energy loss of the jets will be proportional to the amount of plasma the jets traverse. The QGP state is maintained for a short period of time $(10\,\text{fm/c})$, as long as the density and temperature is high enough. When the density decreases, the partons hadronize, cease to interact, and the *freeze out* stage is reached. From this stage, the hadrons are detected in the surrounding detector. The existence of the intermediate liquid QGP phase can only be proven by looking at the momentum distribution of the detected particles.

Transverse momentum

To provide evidence for the QGP, one analyzes the distribution of the hadrons during the *freeze out* phase. In order to do this in a sophisticated manner, one must carefully determine the reference frame and its coordinates. First of all, the z-direction is set to be along the beam axis. Accordingly, one divides the momentum of the participating particles into transverse momentum, p_t and longitudinal momentum, p_z. The transverse momentum is defined as the fraction of the total momentum carried in the xy-plane, i.e

$$p_t = \sqrt{p_x^2 + p_y^2} \tag{1}$$

and similarly, the longitudinal momentum is the momentum along the z-direction. The impact parameter vector is defined in the xy-plane as the distance between the centres of the two participating nuclei. The reaction plane is defined as the plane spanned by the impact parameter parallel to the beam axis, presented in Figure 4. The associated reaction plane angle, ψ_r is defined as being the angle between the reaction plane and the x-axis, $(0 \leq \psi_r \leq \pi)$.
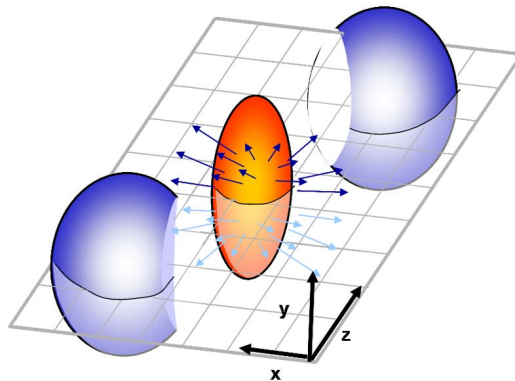

Figure 4: Two colliding nuclei and the overlap region in the xy-plane [11]

A way to define the amount of momentum carried along the beam axis is through the

rapidity:

$$y = \frac{1}{2} \ln \left(\frac{E + p_z}{E - p_z} \right). \tag{2}$$

Depending on how much of the projected areas of the participating nuclei overlap, the hydro-dynamical effects of the plasma vary. It is thus of relevance to make the distinction between the participating and spectator particles, presented in Figure 5. This distinction results in different centrality classes, where high percentage centrality corresponds to peripheral collisions and low percentage centrality corresponds to central collisions [1].
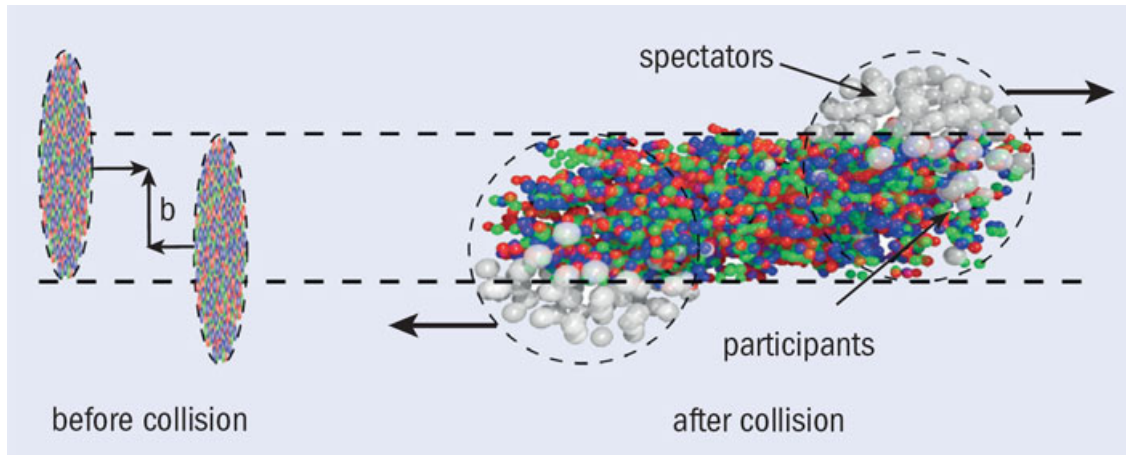

Figure 5: The impact parameter b is related to the centrality. The participants are those affected by the collision whereas the spectator particles remain unaffected. [16]

Chapter 3: Flow

The theory of flow in heavy ion collisions have been developed over the last 20 years. In this section the reasoning that leads to the hydrodynamical description of the QGP is presented.

Fourier expansion of azimuthal particle distributions

It has been proposed that the QGP formed in a heavy ion collision can be described as a fluid, and according to hydrodynamics, *flow* is a collective behaviour of a fluid. In 1994, Voloshin and Zhang suggested in a paper [2] that the azimuthal distribution of particles from the *freeze out* phase can be described with a Fourier expansion. The azimuthal angle ϕ is the angle spanned by the reference direction (z-direction) and a point of interest. Denoting the azimuthal distribution function by $r(\phi)$, the following expression holds for a periodic function:

$$r(\phi) = \frac{x_0}{2\pi} + \frac{1}{2\pi} \sum_{n=1}^{\infty} [x_n \cos(n\phi) + y_n \sin(n\phi)]. \tag{3}$$

The Fourier coefficients x_n and y_n are in turn expressed as integrals weighted over $\cos(n\phi)$ and $\sin(n\phi)$ respectively. For finitely many particles, the integral becomes a sum over the particles ν, with the associated azimuthal angle ϕ_ν:

$$x_n = \int_0^{2\pi} r(\phi)\cos(n\phi)d\phi = \sum_\nu r_\nu \cos(n\phi_\nu) \tag{4}$$

$$y_n = \int_0^{2\pi} r(\phi)\sin(n\phi)d\phi = \sum_\nu r_\nu \sin(n\phi_\nu). \tag{5}$$

Each Fourier coefficient, x_n and y_n, can be associated with a corresponding harmonic or anisotropy parameter v_n, defined as $v_n = \sqrt{x_n^2 + y_n^2}$, and the angle ψ_n $(0 \leq \psi_n \leq 2\pi/n)$ which is the reaction plane angle of the of the "n-th type" flow. The v_n are the flow coefficients, where n denotes the order of the harmonics. Consequently the Fourier coefficients can be expressed as a function of the flow coefficients in the following way [2]:

$$x_n = v_n \cos(n\psi_n) \tag{6}$$

$$y_n = v_n \sin(n\psi_n). \tag{7}$$

Each order of the harmonics describes a hydrodynamical effect, i.e a collective behaviour of the partons, where the coefficients v_n are the different values of the magnitude of the flow. The first order harmonic coefficients x_1 and y_1 are associated with a shift of the distribution in the transverse plane with the related coefficient v_1, which is called the directed flow. The second order flow coefficient v_2 is associated with an elliptic shape, and is hence called elliptic flow [2]. The third order flow coefficient v_3 is associated with a triangular distribution and is hence called triangular flow. The elliptic and triangular distributions are presented in Figure 6. Furthermore, there are anisotropic distributions associated with the flow coefficients v_4, v_5 and v_6. The even coefficients v_2 and v_4 are mainly due to geometrical shape of the plasma, whereas the odd coefficients v_1, v_3 and v_5 are due to fluctuations of the plasma.
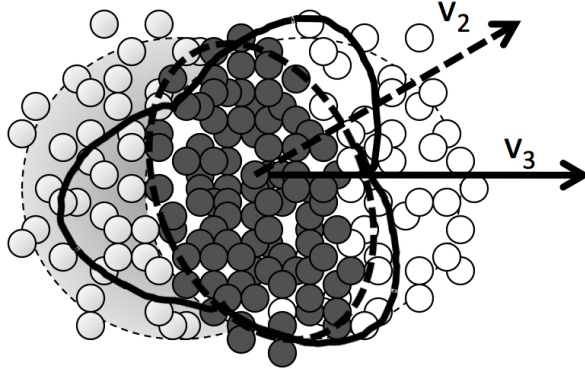
Figure 6: A schematic view of the parton distribution associated with the elliptic flow v_2 and the triangular flow v_3 in the overlap region of colliding nuclei. [12]

Due to spatial reflection symmetry, the sine terms in Equation 3 vanish. The $r(\phi)$ function can be translated to the observed azimuthal anisotropy N, decribed by the triple differential distribution given by the Fourier series

$$E\frac{d^3N}{d^3p} = \frac{1}{2\pi}\frac{d^2N}{p_T dp_T dy}\left(1 + 2\sum_{n=1}^{\infty}v_n(p_T)\cos[n(\phi - \psi_r)]\right) \qquad (8)$$

where ψ_r is the reaction plane angle, ϕ- the azimuthal angle of the detected particles and y- the rapidity relative to the beam axis. The flow coefficients $v_1 - v_5$ can thus be expressed as [2]:

$$v_n = \langle\cos[n(\phi - \psi_r)]\rangle. \qquad (9)$$

Chapter 4: Heavy Ion Collisions at the LHC

Heavy ion research is conducted at the Large Hadron Collider (LHC) at CERN (The European Organization for Nuclear Research) on the Franco-Swiss border and at the Relativistic Heavy Ion Collider (RHIC) at Brookhaven National Laboratory (BNL), situated near New York. This thesis will treat data originating from the ALICE project at CERN, hence this section will serve as an introduction to the the LHC and the experimental tools needed for the conduction of heavy ion research.

The LHC

The Large Hadron Collider is an accelerator with colliding beams and is currently the largest collider at CERN and also in the world. Protons and lead ions are accelerated by a linear pre-accelerator before entering the cyclic accelerator, where the charged nuclei are focused by strong magnetic fields. The momenta of the orbiting nuclei are proportional to
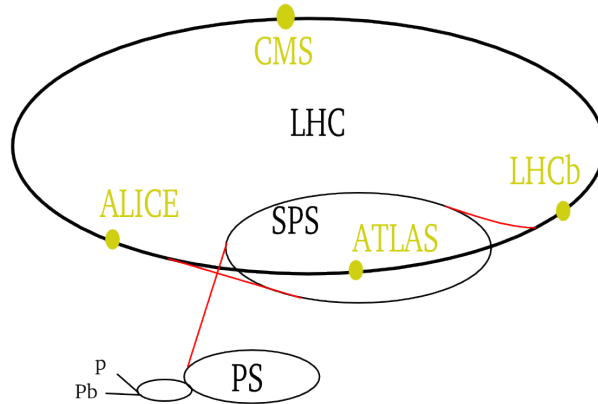
Figure 7: The LHC ring with pre-accelerators and the four main detectors indicated [15].

the strength of the magnetic field and the radius of curvature. Since there is a limitation in the superconducting coils inducing the magnetic fields, one must increase the radius of curvature in order to obtain high momentum of the orbiting particles. This is the reason why the LHC has a circumference of 27 km. This enables the beams of particles to reach a center of mass-energy of $\sqrt{s} = 8$ TeV for proton-proton collisions and a center of mass-energy of $\sqrt{s} = 2.76$ TeV for lead-lead collisions (per nucleon pair). In the near future, the LHC will reach energies of $\sqrt{s} = 13 - 14$ TeV for proton-proton collisions and $\sqrt{s} = 5.5$ TeV for lead-lead collisions. The construction of the LHC was completed in 2008 and it has been running routinely since 2010.

ALICE

There are seven detector experiments at the LHC, all dedicated to certain fields of exploration. ALICE is an acronym for A Large Ion Collider Experiment and is the name of the detector devoted to the conduction of heavy ion research. In the LHC, the highly energetic nuclei beams are accelerated in opposite directions until they collide inside the ALICE detector. As assumed in the previous section, the QGP created in the collision will dynamically evolve in three dimension before the *freeze out*-phase is reached and the partons hadronize. The hadrons and leptons will be detected in the Time Projection Chamber as tracks. A simplified model of the ALICE TPC is presented in Figure 8.

Time Projection Chamber

The Time Projection Chamber (TPC) is a powerful detection instrument that enables the tracking of charged particles in three dimensions. The TPC utilizes the two dimensional

tracking features of the multi-wire proportional chamber (MWPC), and the z-coordinate (along the beam-axis) is determined from the drift time. The principle behind the detection is to let the particles traverse a gas filled container and measure the ionization of the gas by anode wires. One has to take into account that the ionized electrons will need some time to drift to the anodes, which is the principle of the drift chamber. The exact trajectory of the particles in the xy-plane can be established by the wires and the z-direction can be established by the drift time if the drift velocity is known. The momentum of the particles can be computed through the curvature of the particle trajectories induced by an external magnetic field.
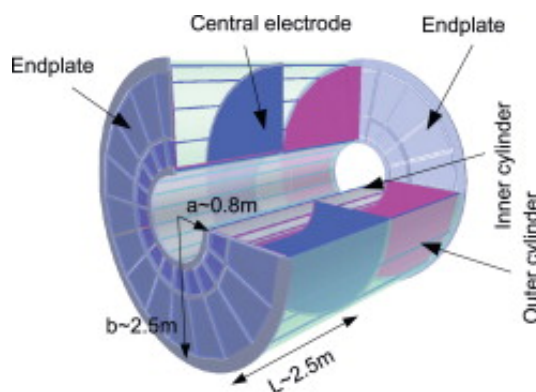

Figure 8: A simplified picture of the structure of the ALICE TPC [13].

Chapter 5: Analysis Method

The aim of this thesis is to study the different kinds of flow by measuring the associated Fourier coefficients, presented in Chapter 3. The idea is to extract information obtained from the actual collisions. As explained in the previous section, the Time Projection Chamber enables detection of particles with a three dimensional reconstruction of the trajectories, as well as an estimate of the momentum of the particles. The data used are stored as several thousand events, each containing tracks corresponding to a detected particle. Each track contains information about the particle, such as the azimuthal angle ϕ and the momentum. In order to compute the flow coefficients, two methods are proposed that extract information about the collisions through the tracks. The two methods are the Event Plane Method and the study of particle correlations, both described below.

The Event Plane Method

The reaction plane cannot directly be extracted from the collisions, therefore one has to construct an event plane for the computation of the flow coefficients. In the Fourier ex-

pansion of the azimuthal distribution introduced in the second chapter, Equation 8, the reaction plane angle ψ_r is used:

$$E\frac{d^3N}{d^3p} = \frac{1}{2\pi}\frac{d^2N}{p_T dp_T dy}\left(1 + 2\sum_{n=1}^{\infty} v_n(p_T, \eta)\cos[n(\phi - \psi_r)]\right).$$

The reaction plane angle will be replaced by the event plane angle ψ_n defined through

$$\psi_n = \frac{1}{n}\arctan\left(\frac{\sum_i \sin(n\phi_i)}{\sum_i \cos(n\phi_i)}\right) \tag{10}$$

where n is the n-th harmonic and ϕ_i is the lab azimuthal angle of the i-th particle. The event plane angles ψ_1 to ψ_5 are used in the determination of the flow coefficients v_1 to v_5. The ψ_1 event plane angle ranges the whole the detector, $\left(-\frac{\pi}{2}, \frac{3\pi}{2}\right)$. The ψ_2 event plane angle is constructed in the region $\left(-\frac{\pi}{2}, \frac{\pi}{2}\right)$, the ψ_3 is constructed in the region $\left(-\frac{\pi}{3}, \frac{\pi}{3}\right)$ and so on. The constructed event planes are used for the computation of the flow coefficients following the method presented in the subsequent chapter regarding computation.

Dihadron Correlation

Assuming flow effects are present in s, one can argue for the existence of pair-wise correlations, i.e the probability for detecting a particle with a certain momentum and azimuthal angle ϕ_1 is dependent on the probability for detecting another particle with a certain momentum and azimuthal angle ϕ_2. Following the line of reasoning presented below:

$$\begin{aligned}
\langle\cos[n(\phi_1 - \phi_2)]\rangle &= \text{Re}\langle e^{in(\phi_1 - \phi_2)}\rangle \\
&= \text{Re}[\langle e^{in(\phi_1 - \phi_2 + \psi_r - \psi_r)}\rangle] \\
&\simeq \text{Re}[\langle e^{in(\phi_1 - \psi_r)}\rangle\langle e^{-in(\phi_2 - \psi_r)}\rangle] \\
&\simeq \langle\cos[n(\phi_1 - \psi_r)]\rangle\langle\cos[n(\phi_2 - \psi_r)]\rangle \\
&= v_2 v_2 \\
&= v_2^2
\end{aligned} \tag{11}$$

one can argue that it suffices to study the azimuthal angles of two particle correlations in order to compute the flow coefficients. ϕ_1 and ϕ_2 are the azimuthal angles of two particles, only correlated through their common correlation to the reaction plane. Upon observation, it is evident that only the ϕ_1 and ϕ_2 angles are needed, i.e for this method the event plane needs not be computed [5]. By defining an angle $\Delta\phi = \phi_1 - \phi_2$ one computes the v_n by constructing the average of the cosine of the $\Delta\phi$:

$$v_n^2 = \frac{\sum_{i=1}^{N}\cos(n\Delta\phi)}{N}. \tag{12}$$

Computation

The analysis in this thesis has been made from software written in C++ which utilizes the ROOT framework [8]. The data is extracted from Pb-Pb collisions at the LHC at a center of mass energy $\sqrt{s_{NN}} = 2.76\,\text{TeV}$, for the rough impact parameter range of 10-20%. The number of events is $247\,981$.

The Event Plane Method

A pre-written code for the computation of the 2nd order event plane was used as a starting point, and extended to v_1, v_3, v_4 and v_5. The azimuthal angles ϕ_i were obtained by extracting the primary tracks associated with a transverse momentum distribution of $0.5 < p_T < 3.0\,\text{GeV/c}$. The event plane was constructed according to Equation 10 for 10-20 % centrality using a statistical sample of $247\,981$ events. The reconstructed event plane is presented in Figure 12. Once the event plane has been established, the azimuthal distribution of the particles with respect to the reaction plane was visualized by constructing a histogram with the difference in the azimuthal angle and the event plane angle ϕ-ψ_n as a function of the transverse momentum p_T. This was done for ψ_1-ψ_5 and is presented in Figure 13 in the Appendix. The actual flow coefficients v_n were computed by first of all introducing the fit curve

$$f_n = 1 + 2v_n \cos[n(\phi - \psi_n)] \tag{13}$$

which originates from Equation 8, and extracting the shape of the distributions obtained above. This is the distribution of the azimuthal angle relative to the measured event plane angle, and is presented in Figures 14-18. Choosing the argument of the cosine term in Equation 13 to obtain a maximum value, the following equation is constructed:

$$v_n = \frac{f_{1,max} - 1}{2}. \tag{14}$$

The v_n values can be obtained from Equation 14, meaning that the flow coefficients are correlated to how the azimuthal distribution follows a perfect $1 + \cos[n(\phi - \psi_n)]$ modulation. The v_n coefficients can be plotted as a function of the transverse momentum presented in Figure 9. The statistical errors in the event plane method are computed through the method of least squares. What we expect to see is that at low p_T the dominant correlations are through the common event planes, while at high p_T we observe dijet produced correlation, e.g. jet fragmentation.

Dihadron Correlations

For the study of the dihadron correlations, a code was written. The idea was to chose a small range of momentum, and choose the azimuthal angles ϕ_1 and ϕ_2. First of all, the $\Delta\phi$ distribution was plotted. Following the line of reasoning presented in the previous chapter,

in Equation 11 and Equation 12, the v_n coefficients were computed as the mean of the cosine of the angular difference $\Delta\phi$:

$$v_n = \sqrt{\frac{\sum_{i=1}^{N} \cos(n\Delta\phi)}{N}}.$$ (15)

It has been taken into account in the computation that the pair of trigger and associated particles should not be counted twice. For the estimation of the statistical errors, the deviation of the v_n^2 in Equation 12 is easily computed through

$$\delta v_n^2 = \sqrt{\langle v_n^4 \rangle - \langle v_n^2 \rangle^2}$$ (16)

and the δv_n^2 is related to δv_n in the following way

$$(v_n - \delta v_n)^2 = v_n^2 - 2 v_n \delta v_n + \delta v_n^2$$ (17)

since $\delta v_n^2 \simeq 0$ the δv_n can be expressed as:

$$\delta v_n \simeq \frac{\delta v_n^2}{2 v_n}$$ (18)

Each v_n coefficient is computed with this method by scanning the p_T region $0 < p_T < 6\,\mathrm{GeV/c}$ in steps of $0.2\,\mathrm{GeV/c}$. The distribution of $\Delta\phi$ is plotted for the $0 < p_T < 6\,\mathrm{GeV/c}$ region, divided into steps of $0.2\,\mathrm{GeV/c}$ in Figures 19, 20 and 21. The values of v_n are computed for each region, and plotted together with the results from the event plane method in the subsequent chapter.

Chapter 6: Results

The two methods, the event plane method and the dihadron correlations, have been used in this thesis to study different kinds of flow. Below are the results from the two methods presented, followed by a comparison in the subsequent chapter.

The Event Plane Method

The results from the event plane method for the five flow coefficients are presented in Figure 9. In this region $0 < p_T < 6\,\mathrm{GeV/c}$, the error bars are negligible. This is due to the construction of the event plane, which was done for a region of $0.5 < p_T < 3\,\mathrm{GeV/c}$, a region with a great deal of statistics. As a reference, the elliptic flow coefficient v_2 is presented in Figure 10 where the transverse momentum ranges from 0 to 20 GeV/c and the error bars become apparent at high p_T. The response in the high p_T regions is assumed to originate from the appearance of jets, explained in the second chapter. Hadronic jets are produced in the QGP by collision of the quarks and gluons, often exiting the plasma back

to back. Since the event plane is constructed for a low p_T region, the high p_T response of hadronic jets results in highly energetic tracks with an angular separation of approximately 180°. There will therefore be no contribution to the flow coefficients, and the effect of the di-jets will cancel out with respect to the event plane. This is in accordance with what is seen in Figure 11 as a decrease for higher transverse momentum. The flow coefficients v_1, v_4 and v_5 show a higher distribution in the region of p_T used for the construction of the event planes ($0.5 < p_T < 3\,\text{GeV/c}$), and almost no contribution outside of this region.

Upon examination of the event planes presented in Figure 12 in the Appendix, all ψ_1 to ψ_5 event planes show a rather flat distribution. For a perfect detector, the ψ_1 event plane would provide a completely flat distribution. Since this is not exactly fulfilled in Figure 12, it is suggested to take this imperfection of the detector into account for future studies. For ψ_1, the event plane angle spans the whole region ($-\frac{\pi}{2}$, $\frac{3\pi}{2}$). For ψ_2, the event plane has been constructed so that it suffices to treat the region ($-\frac{\pi}{2}$, $\frac{\pi}{2}$), which is shown in Figure 12. The ψ_3 and ψ_4 event planes show a peculiar shape, with a drastic decrease around the edges of the event plane. This is due to the binning used in the computation. ψ_3 and ψ_4 span over ($-\frac{\pi}{3}$, $\frac{\pi}{3}$) and ($-\frac{\pi}{4}$, $\frac{\pi}{4}$), respectively. All computation has been made by using the binning of 20 bins covering 2π. This means that the first and last bin will contain a third of the information for ψ_3 and half the information for ψ_4. This is exactly what is on display in Figure 12. The ψ_5 event plane spans over ($-\frac{\pi}{5}$, $\frac{\pi}{5}$) and will thus cover all 4 bins.

The fit curves in Figures 14 to 18 are used to extract the values for v_1 to v_5. For low p_T they provide a smooth distribution with negligible errors, and the error bars increase for values of p_T higher than that used for the construction of the event planes ($p_T = 3\,\text{GeV/c}$).
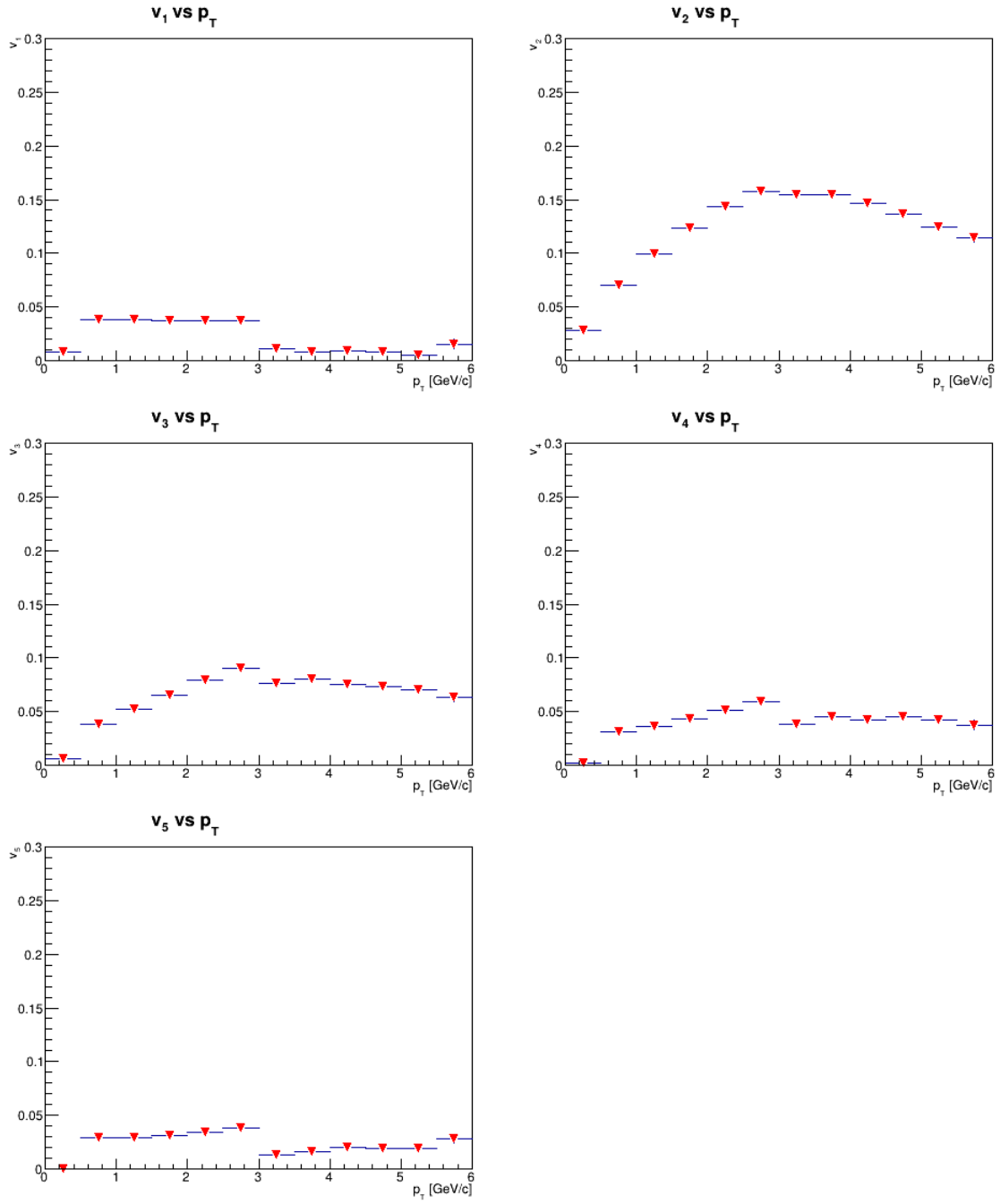
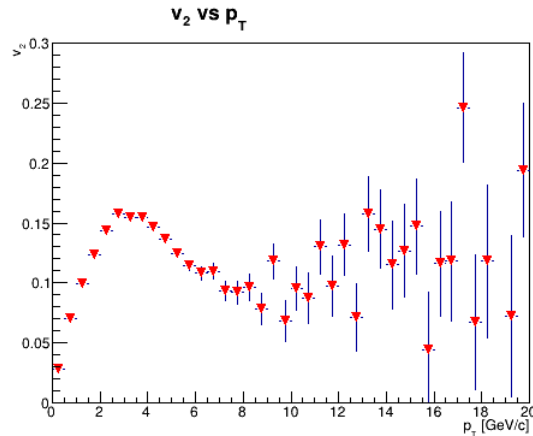Figure 9: $v_1 - v_5$ at $0 < p_T < 6\,\mathrm{GeV/c}$ calculated with the event plane method.

Figure 10: v_2 at $0 < p_T < 20\,\mathrm{GeV/c}$ calculated with the event plane method.

Dihadron Correlations

The results from the dihadron correlations are presented in Figure 11 alongside the results from the event plane method, for a comparison. The general trend for the flow coefficients calculated through the dihadron correlations is the drastic increase for high values of the transverse momentum. This effect can on the one hand be explained by the lack of statistics when approaching higher values of the transverse momentum. On the other hand, it can be explained by jets. The reaction plane is the plane spanned by the flow participants. For high p_T there will be few tracks corresponding to highly energetic jets, which means that the reaction plane will be spanned by the back to back tracks with angular separation of approximately 180°. This results in a very high correlation, that provides high values of the flow coefficients. The directions of the jets in the collision are arbitrary with respect to the reaction plane. Although this holds, the jets are affected by the plasma through jet quenching, and their momentum will be reduced proportional to the amount of plasma they traverse. For example, a non-central collision would provide a geometric overlap region with an almond shape with its short axis in the reaction plane, [4] resulting in highly energetic jets exiting mainly in the direction of the reaction plane. In this central collision (10-20% centrality), this effect is still valid, even though not as dominant as for non central collisions. This explains why the jets also seem to follow the collective phenomenon of flow, even though it originates from jet quenching. The actual dihadron correlations are presented in Figures 19, 20 and 21 in the Appendix. For a large amount of statistics, i.e for the tracks obtained at low transverse momentum, the correlations provide a smooth distribution with negligible error bars. The correlations become irregular for p_T over $4\,\mathrm{GeV/c}$, also revealing the lack of statistics and the few highly energetic jets.
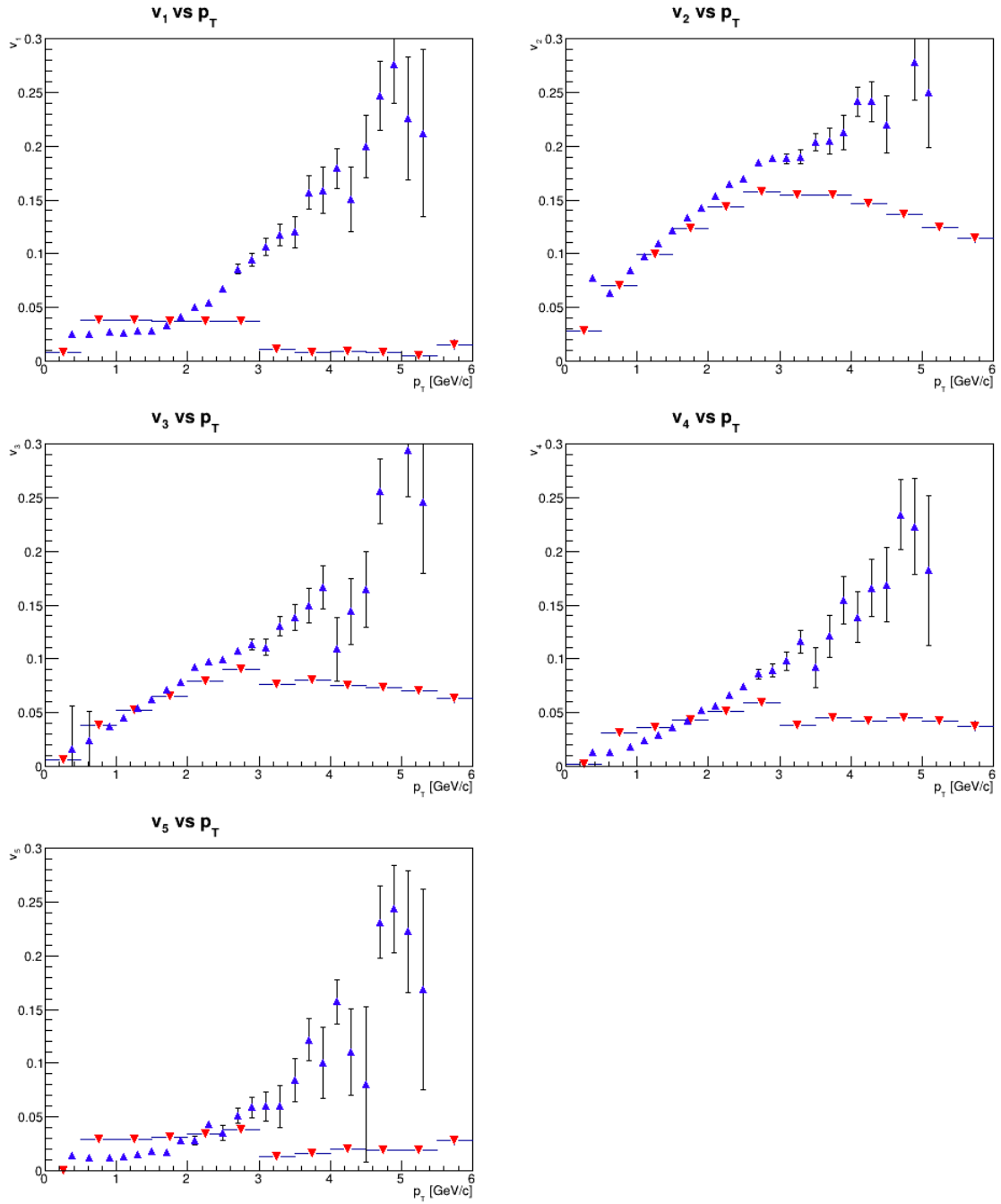
19

Figure 11: $v_1 - v_5$ at $0 < p_T < 6\,\mathrm{GeV/c}$ calculated with the event plane method (red), and the particle cumulant method (blue).

Chapter 7: Conclusion

In this thesis, the flow effects of the QGP have been studied. The particle azimuthal distribution in lead-lead collisions have been shown to be anisotropic, implying the existence of *flow*. It is evident that the dominant contribution is that of the elliptic and triangular flow, being significantly larger than that corresponding to the flow coefficients v_1, v_4 and v_5. This is in accordance to what is expected in this type of central collisions (10-20% centrality), even though the dominant v_2 and v_3 effect would be larger for more non-central collisions. Recent results from an experiment made at the ATLAS detector at CERN for $\sqrt{s_{NN}} = 2.76$ TeV lead-lead collisions show similar patterns using the two methods presented above, with dominant elliptic flow for 10-20% centrality [7].

Regarding the two methods used, they provide similar results for low values of the transverse momentum, whereas they differ significantly when approaching higher values. In the low p_T region, the methods' agreement can be interpreted as a success in describing collective flow. The differences between the two methods should not be interpreted as a failure and that the methods are incomplete. The deviations can rather be seen directly from the formulation of the two methods. In the event plane method, the number of tracks at low p_T dominate. The event plane method can be interpreted as being *global* whereas the dihadron correlations treat more local effects. The main contribution at high p_T are due to jets originating from hard collisions, and the dihadron correlations treat the jets as very correlated, resulting in large flow coefficients. Both methods provide evidence for anisotropy due to the collective expansion at low transverse momentum, $0 < p_T < 3$ GeV/c, and anisotropy due to path-length dependent jet quenching effect at $p_T > 3$ GeV/c.

In conclusion, both methods are successful in treating the flow effects found in low transverse momentum regions, but the results become harder to interpret in higher p_T regions. The non-constant results for the event plane angle ψ_1 shown in Figure 12 reveal imperfections in the detector, which should be taken into account when analyzing similar data in the future. Using a larger sample of statistics, both methods would presumably provide more accurate results.

Acknowledgements

Appendix

The Event Plane Method

The constructed event planes used in the event plane method are presented in Figure 12.
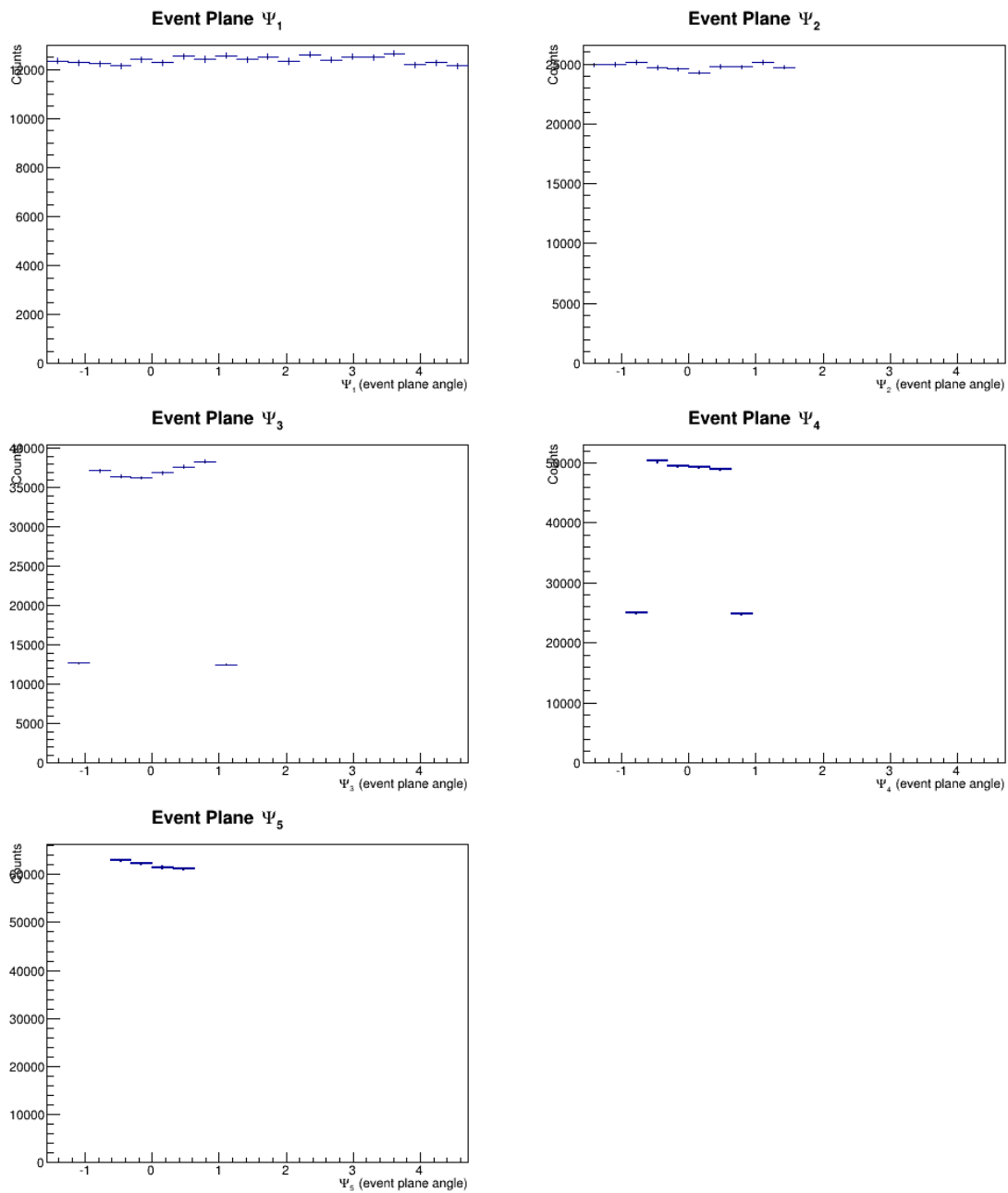

Figure 12: The constructed event planes ψ_1 to ψ_5 used in the event plane method.

Using the event planes constructed above, the transverse momentum p_T is varying with $\phi - \psi_n$ for all event planes ψ_1 to ψ_5 according to Figure 13.
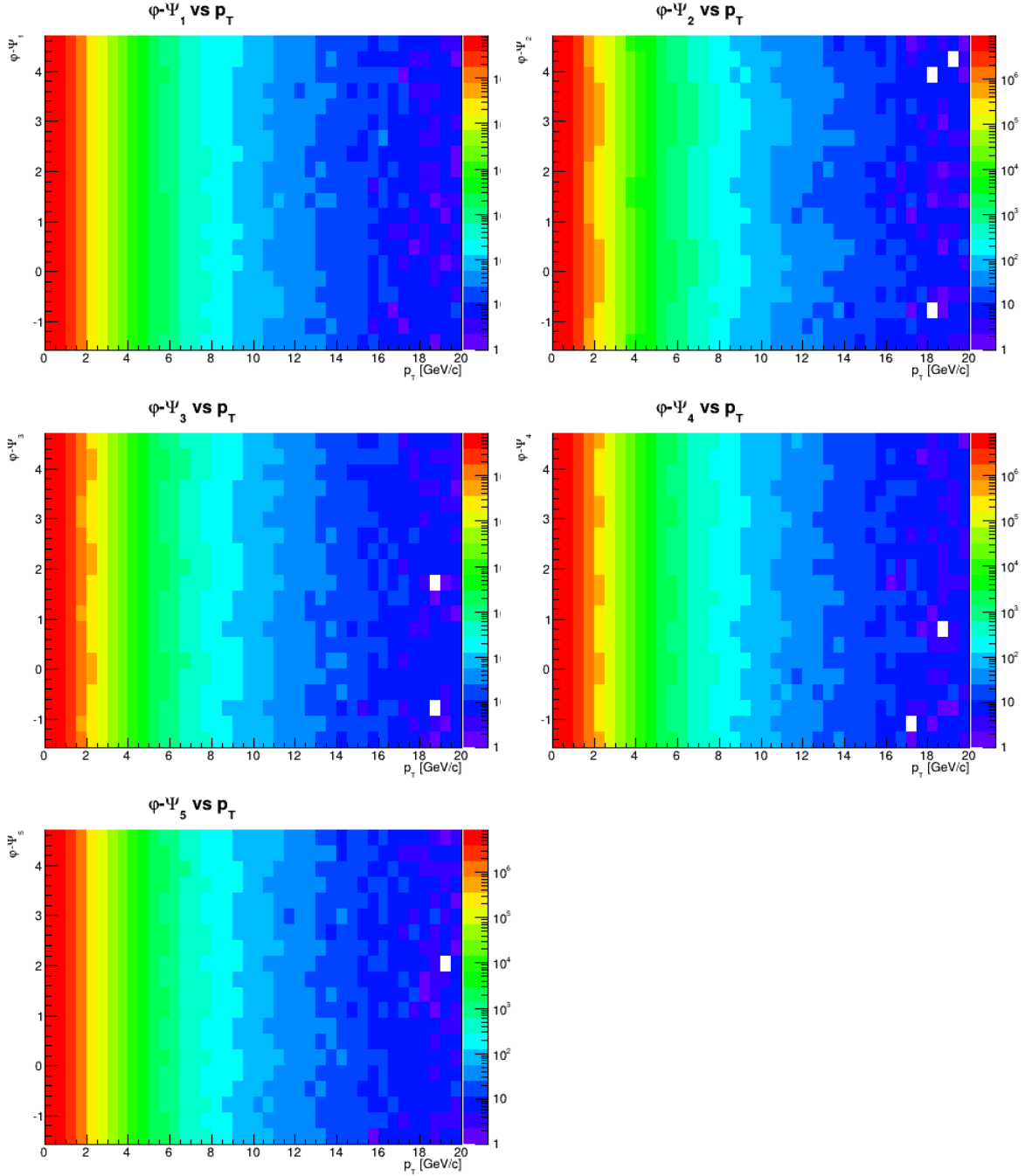

Figure 13: Azimuthal distribution as a function of the constructed reaction plane for v_1 to v_5.

The azimuthal distribution relative to the difference $\phi - \psi_n$ in Figures 14 through 18. The fit is presented for each event plane ψ_1 to ψ_5, for p_T in the regions $0.5 < p_T < 1.0\,\text{GeV/c}$, $3.0 < p_T < 3.5\,\text{GeV/c}$ and $5.5 < p_T < 6.0\,\text{GeV/c}$.
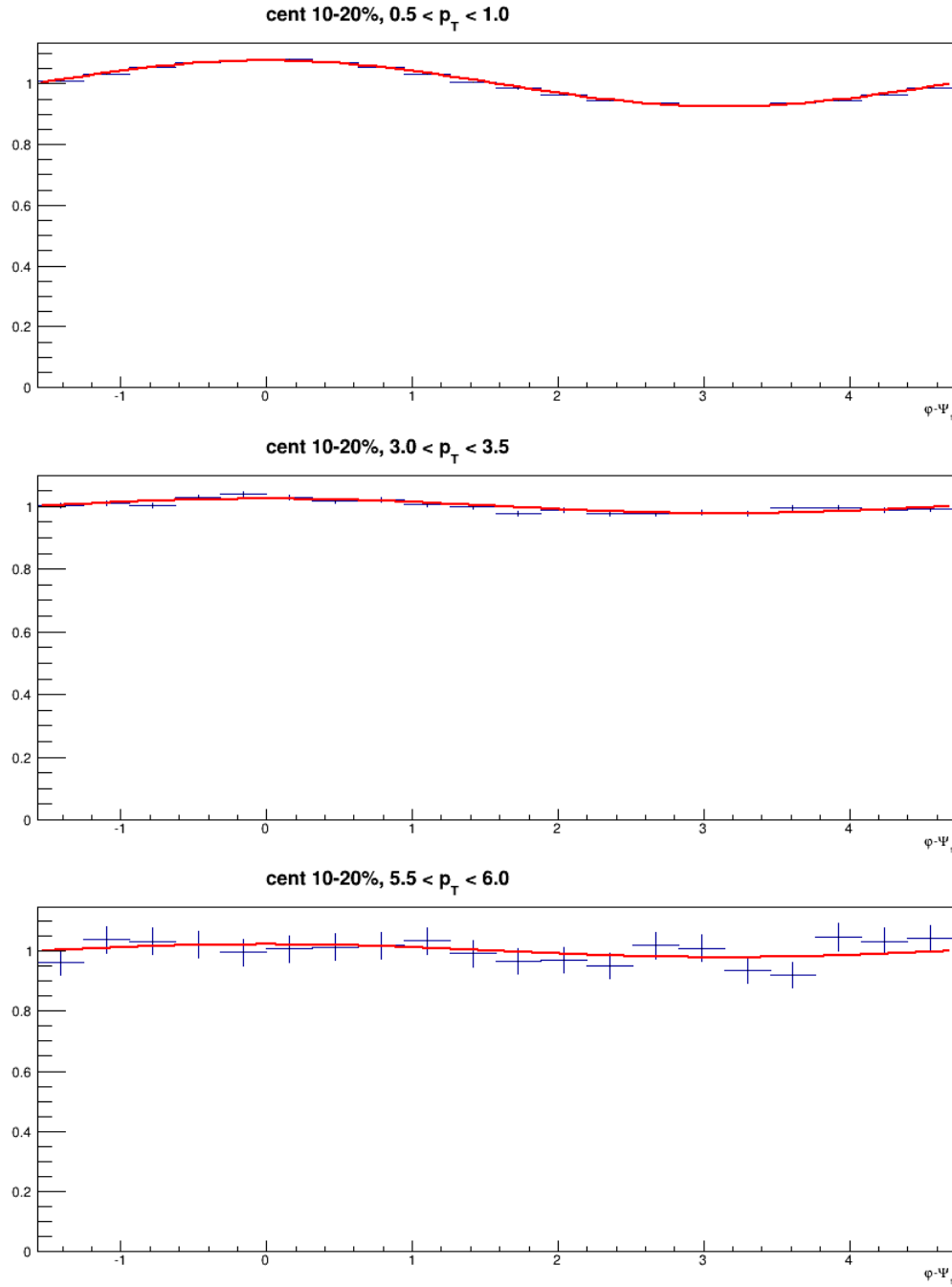
Figure 14: v_1-fit for $0.5 < p_T < 1.0$, $3.0 < p_T < 3.5$ and $5.5 < p_T < 6.0$ GeV/c with the normalized yield on the y-axis
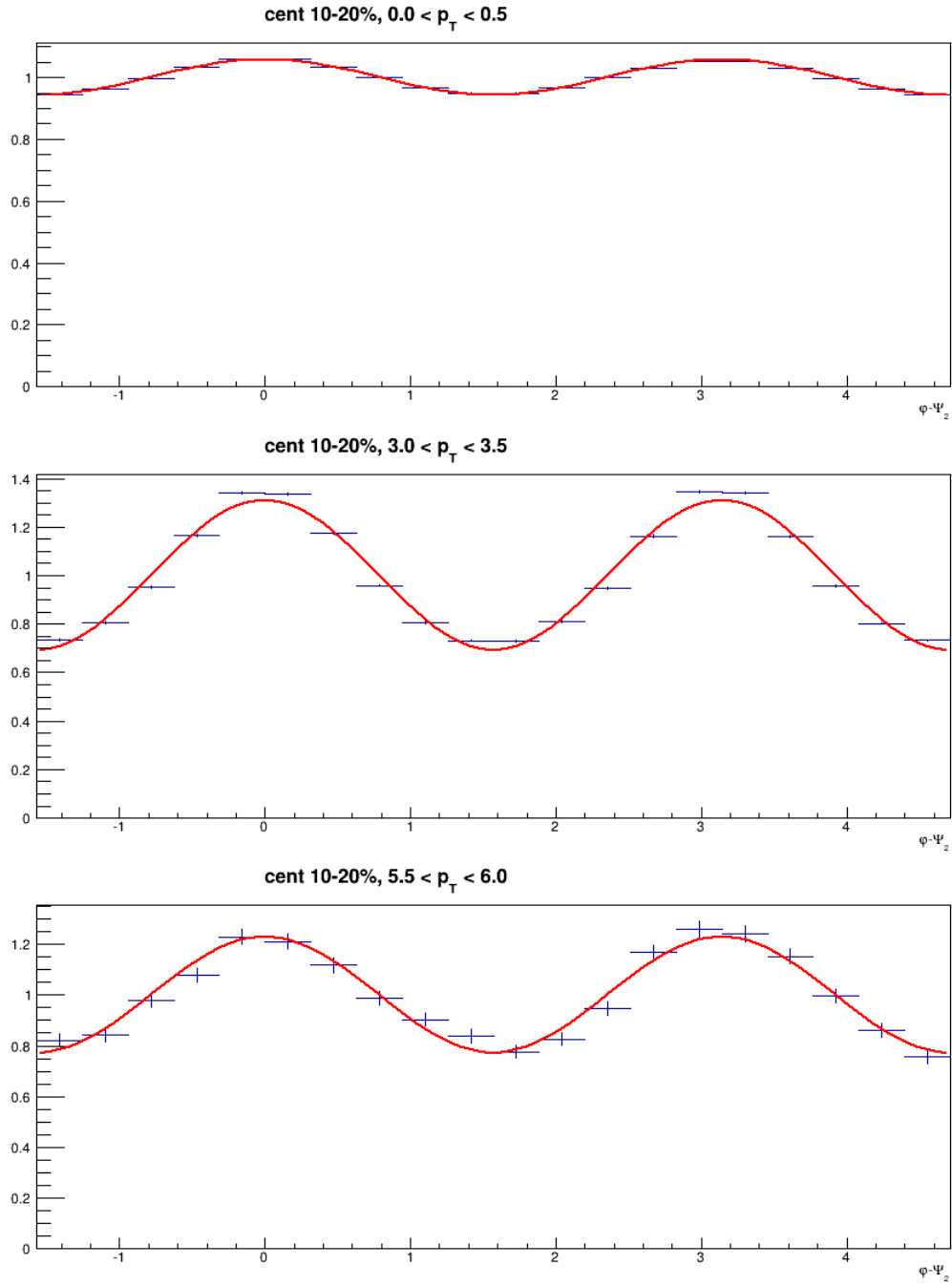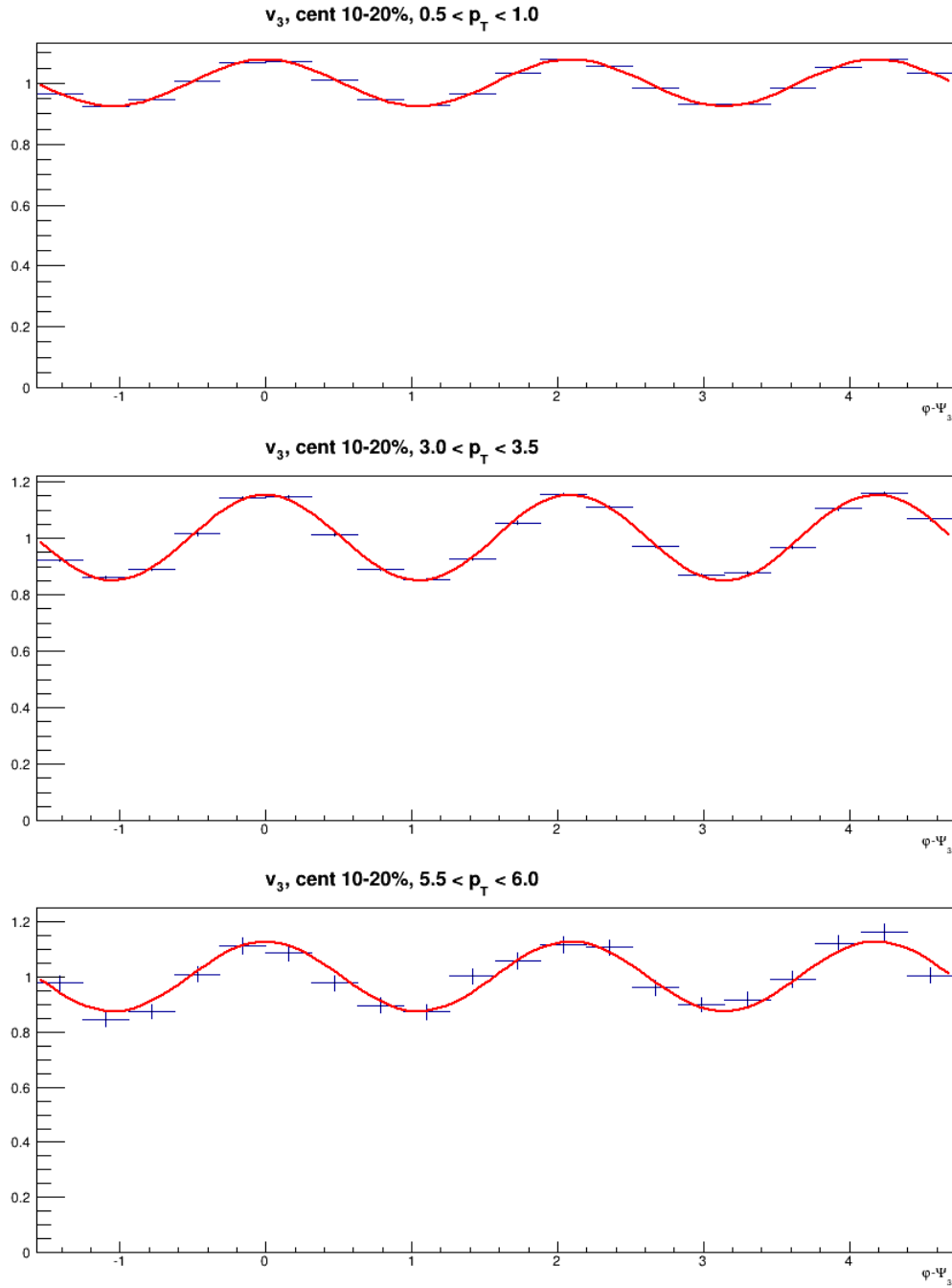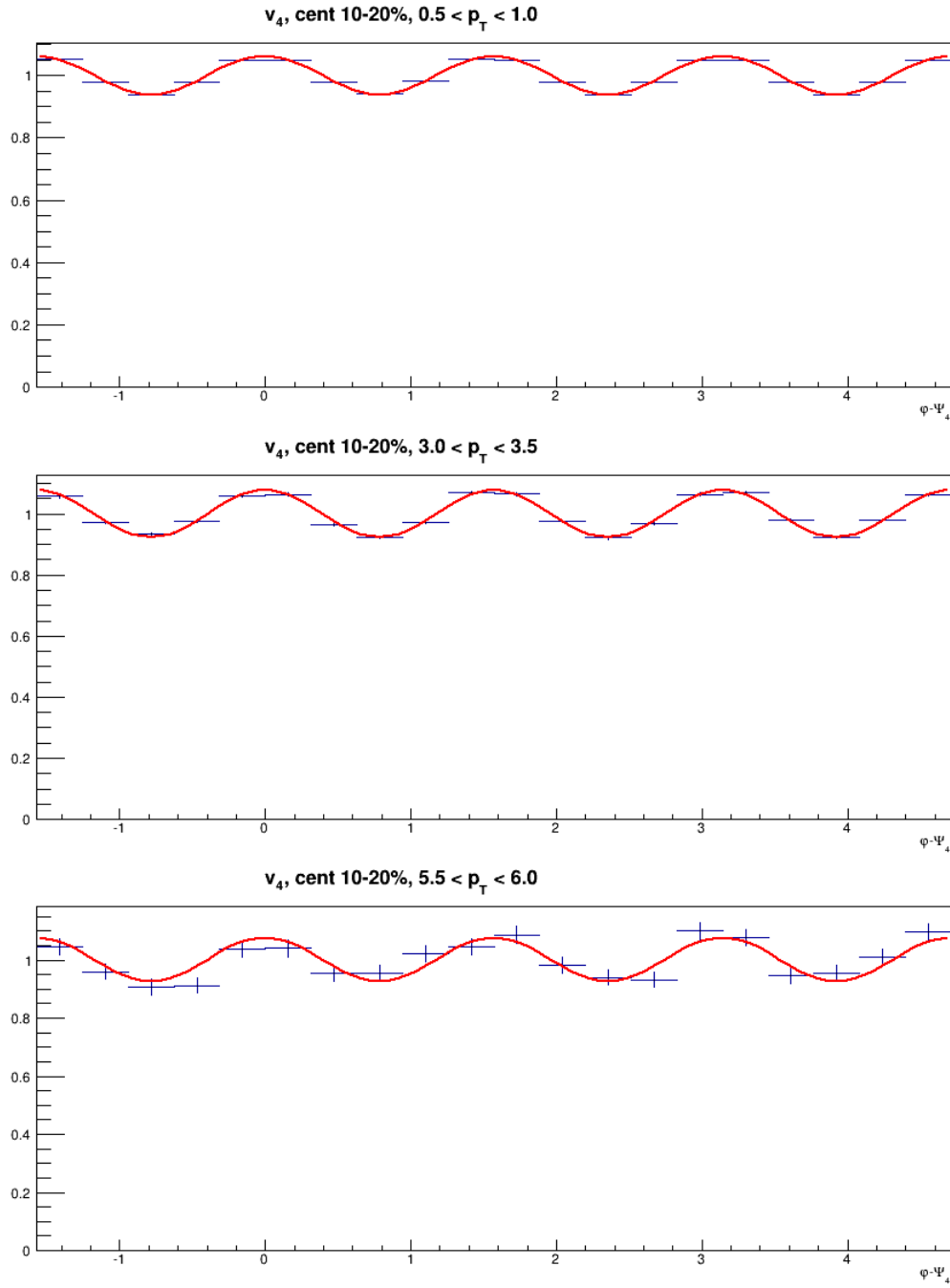
Figure 15: v_2-fit for $0.5 < p_T < 1.0$, $3.0 < p_T < 3.5$ and $5.5 < p_T < 6.0$ GeV/c with the normalized yield on the y-axis

Figure 16: v_3-fit for $0.5 < p_T < 1.0$, $3.0 < p_T < 3.5$ and $5.5 < p_T < 6.0$ GeV/c with the normalized yield on the y-axis

Figure 17: v_4-fit for $0.5 < p_T < 1.0$, $3.0 < p_T < 3.5$ and $5.5 < p_T < 6.0$ GeV/c with the normalized yield on the y-axis
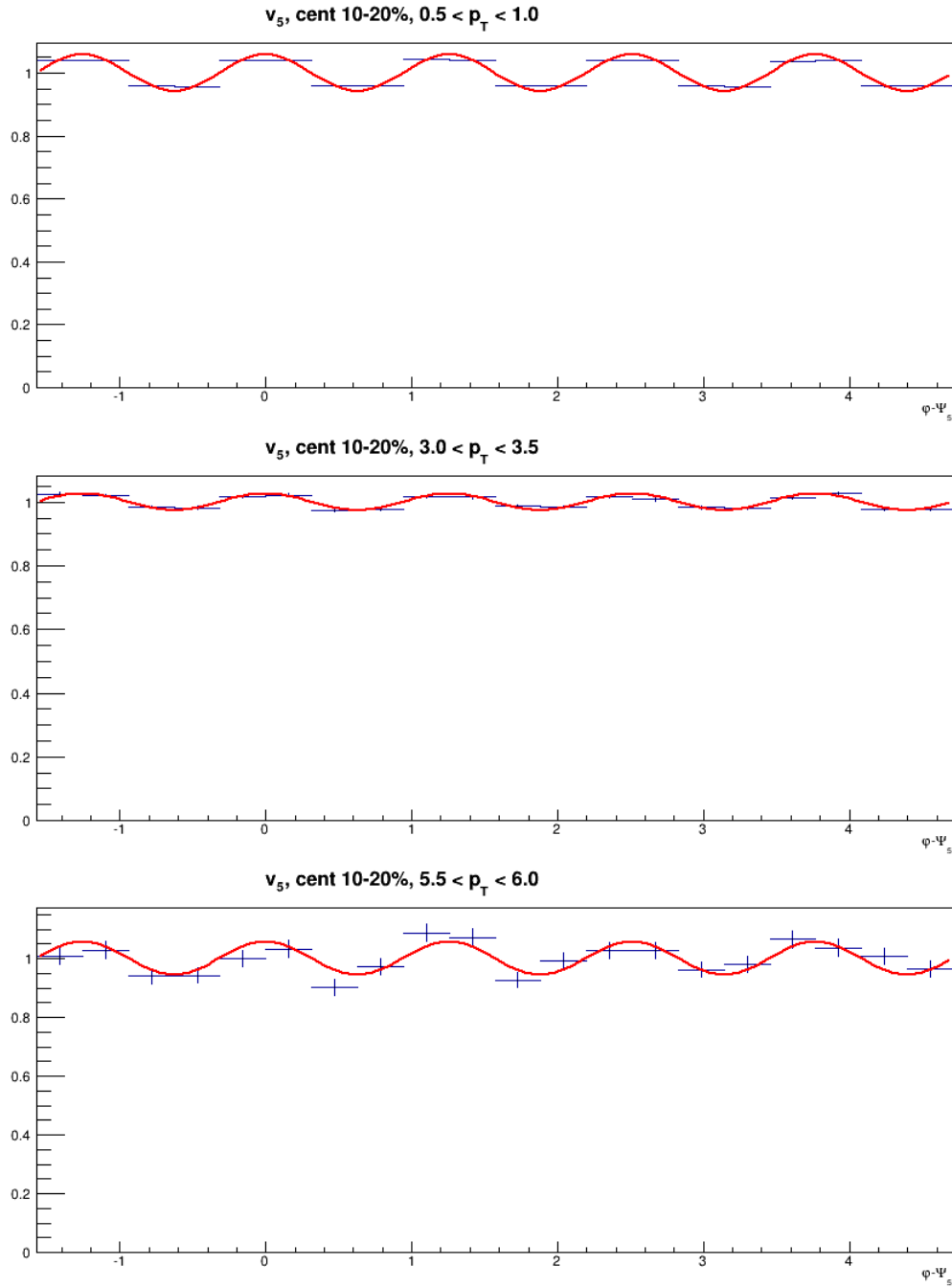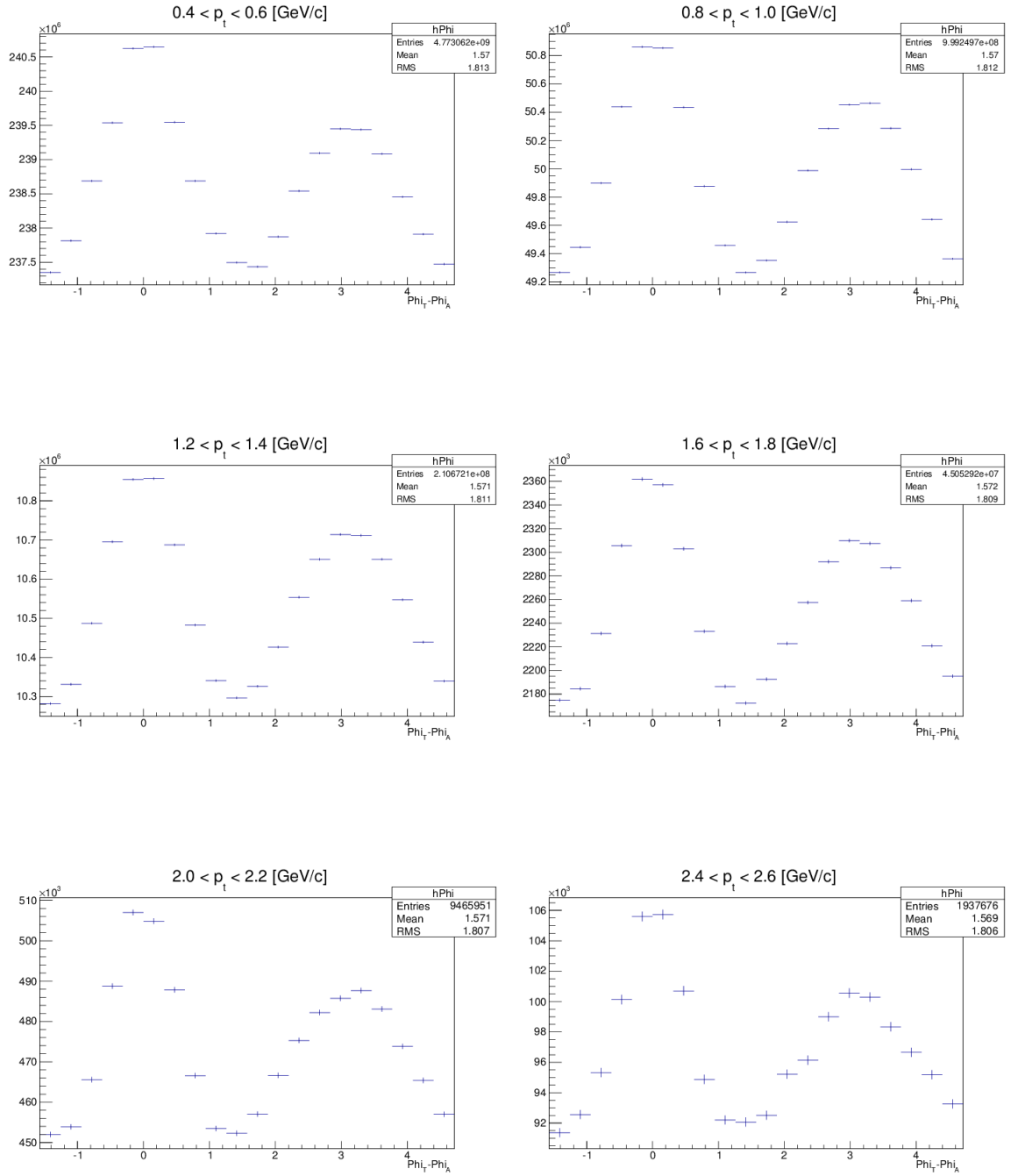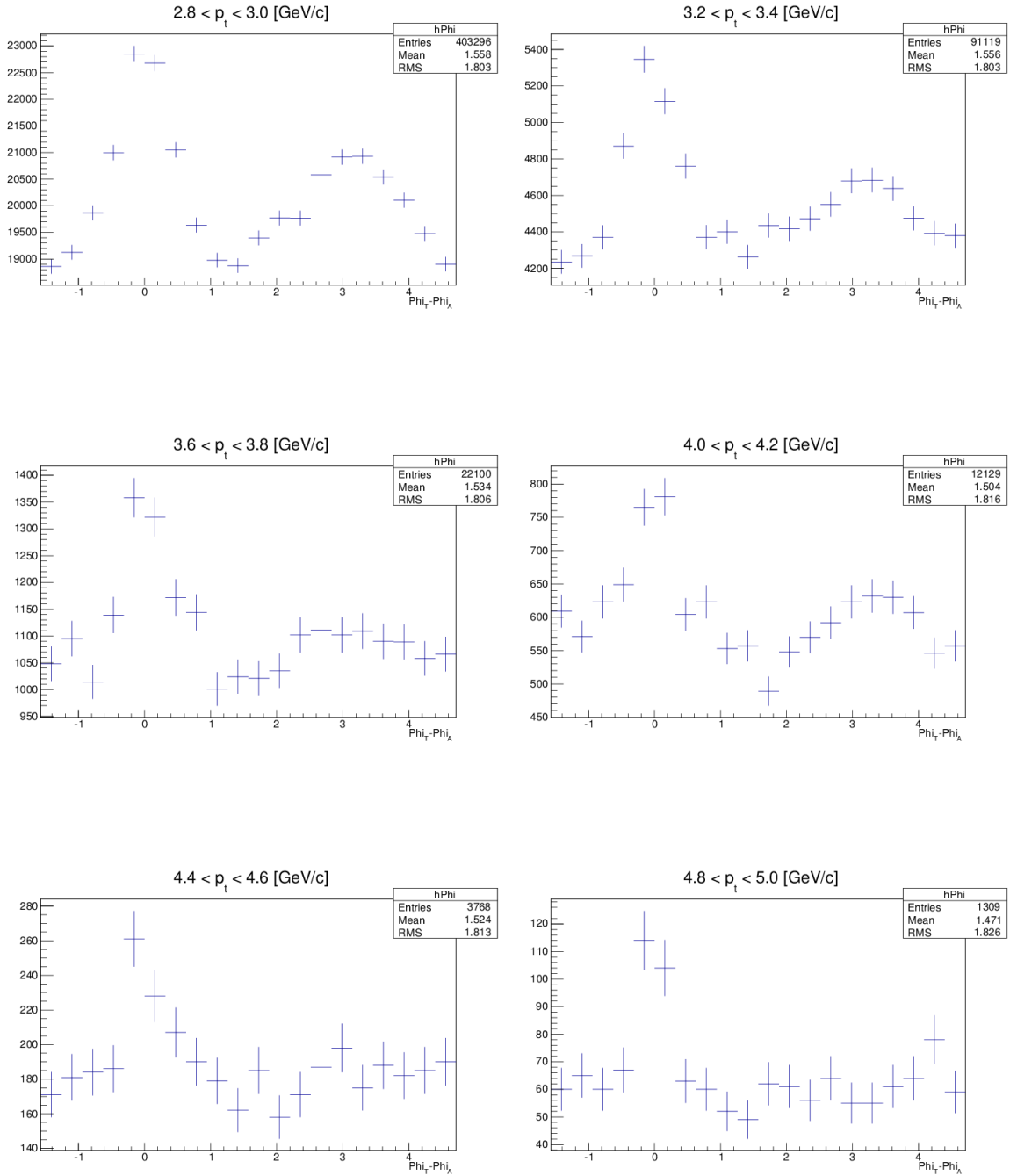
Figure 18: v_5-fit for $0.5 < p_T < 1.0$, $3.0 < p_T < 3.5$ and $5.5 < p_T < 6.0$ GeV/c with the normalized yield on the y-axis

Dihadron Correlations

The dihadron correlations are presented in Figures 19, 20 and 21 as a function of the difference in trigger and associated angles $\Delta\phi$ for $0.4 < p_T < 5.8\,\mathrm{GeV/c}$.

Figure 19: The dihadron correlations for several p_T intervals as a function of $\Delta\phi$.

Figure 20: The dihadron correlations for several p_T intervals as a function of $\Delta\phi$.
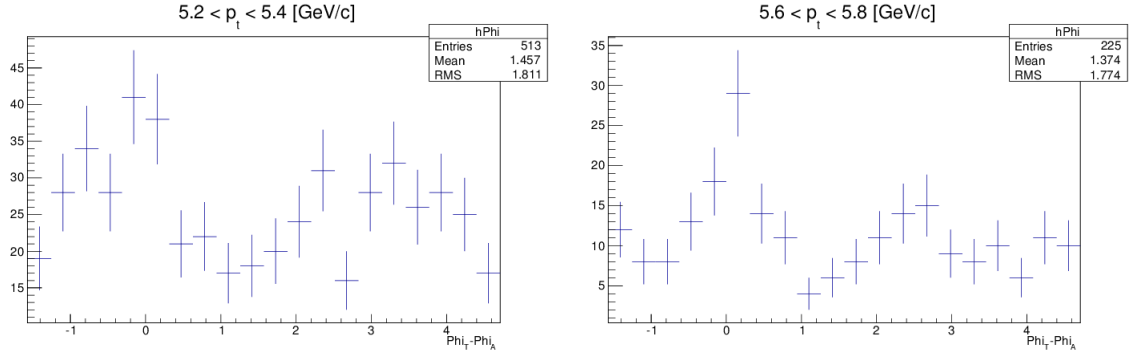
Figure 21: The dihadron correlations for several p_T intervals as a function of $\Delta\phi$.

References

[1] E. Iancu, "QCD in heavy ion collisions," arXiv:1205.0579 [hep-ph].

[2] S. Voloshin and Y. Zhang, "Flow study in relativistic nuclear collisions by Fourier expansion of Azimuthal particle distributions," Z. Phys. C **70** (1996) 665 [hep-ph/9407282].

[3] A. M. Poskanzer and S. A. Voloshin, "Methods for analyzing anisotropic flow in relativistic nuclear collisions," Phys. Rev. C **58** (1998) 1671 [nucl-ex/9805001].

[4] S. A. Voloshin, A. M. Poskanzer and R. Snellings, "Collective phenomena in non-central nuclear collisions," arXiv:0809.2949 [nucl-ex].

[5] M. Luzum, "Collective flow and long-range correlations in relativistic heavy ion collisions," Phys. Lett. B **696** (2011) 499 [arXiv:1011.5773 [nucl-th]].

[6] B. Alver, M. Baker, C. Loizides and P. Steinberg, "The PHOBOS Glauber Monte Carlo," arXiv:0805.4411 [nucl-ex].

[7] G. Aad *et al.* [ATLAS Collaboration], "Measurement of the azimuthal anisotropy for charged particle production in $\sqrt{s_{NN}} = 2.76$ TeV lead-lead collisions with the ATLAS detector," Phys. Rev. C **86** (2012) 014907 [arXiv:1203.3087 [hep-ex]].

[8] http://root.cern.ch/drupal/

[9] http : //en.wikipedia.org/wiki/Parton_28particle_physics29Parton_distribution_functions

[10] http : //sbhep − nt.physics.sunysb.edu/HEP/AcceleratorGroup/1000px−Standard_Model_of_Elementary_Particles.svg.png

[11] http://www.quantumdiaries.org/wp-content/uploads/2011/02/FlowPr.jpg

[12] http://inspirehep.net/record/1112008/files/figv3.png

[13] http : //www.sciencedirect.com/science/article/pii/S0168900210030160

[14] http : //th.physik.uni − frankfurt.de/ scherer/vortrag/HHLR/figures_06/PhaseDiagram.jpg

[15] http : //spotfire.tibco.com/blog/wp − content/uploads/250px − LHC_svg2.png

[16] http://cerncourier.com/cws/article/cern/53089

[17] http://inspirehep.net/record/1094861/plots